New Insights in the Optic Radiations Connectivity in the Human Brain

Alessandro Arrigo,[1] Alessandro Calamuneri,[2] Enricomaria Mormina,[1] Michele Gaeta,[1] Angelo Quartarone,[3] Silvia Marino,[3] Giuseppe Pio Anastasi,[1] and Pasquale Aragona[1]

[1]Department of Biomedical Sciences and Morphological and Functional Images, University of Messina, Messina, Italy
[2]Department of Neurosciences, University of Messina, Messina, Italy
[3]IRCCS Centro Neurolesi Bonino Pulejo, Messina, Italy

Correspondence: Alessandro Arrigo, University of Messina, Department of Biomedical Sciences and Morphological and Functional Images, Via Consolare Valeria, 1 Messina, 98125, Italy; alessandro.arrigo@hotmail.com.

Submitted: August 31, 2015
Accepted: December 4, 2015

Citation: Arrigo A, Calamuneri A, Mormina E, et al. New insights in the optic radiations connectivity in the human brain. *Invest Ophthalmol Vis Sci*. 2016;57:1–5. DOI:10.1167/iovs.15-18082

Purpose. To study optic radiations connectivity by means of advanced magnetic resonance imaging (MRI) approaches, noninvasively, in vivo, in healthy human brains.

Methods. Sixteen healthy subjects (nine males, age range, 25–40 years) were included in this study. Morphologic and diffusion data were acquired by means of a 3T MRI scanner. Using an advanced tractographic technique, based on probabilistic constrained spherical deconvolution algorithm, postprocessing analyses were performed. Statistical analysis was carried out using the 2-tailed Wilcoxon rank sum test. Outcome measure was the percentage distribution of optic radiations streamlines in different cortical visual areas (V1–V5). The latter were detected by means of Juelich probabilistic histologic atlas.

Results. Average connectivity analyses revealed that the optic radiations are mainly distributed in V1 (47.46% ± 5.5) and V2 (32.45% ± 3.98); furthermore, direct connections with V3 (7.81 ± 3.06), V4 (4.22% ± 1.82), and V5 (8.06% ± 2.65) were also detected.

Conclusions. In the present study, the connectivity profile of optic radiations, obtained by means of algorithms not affected by the limitations of other tractographic techniques, such as diffusion tensor imaging, was shown in healthy human brains. Interestingly, direct connections with V4 were detected for the first time in humans; moreover, further support on the possible existence of V5 connections was provided. Our findings showed new connections between lateral geniculate nuclei and cortical visual areas, giving a further possible comprehension of the phenomena leading to the visual signals elaboration.

Keywords: optic radiations, tractography, visual cortex, thalamus/lateral geniculate nucleus, connectivity

Optic radiations are two well-represented white matter fiber bundles which allow direct connection between lateral geniculate nuclei (LGNs) and visual cortex. Each optic radiation is conventionally divided into three different portions: anterior, middle, and posterior.[1] The anterior bundle initially runs anterolaterally near the temporal horn of lateral ventricle and, assuming a posterolateral course, forms the Meyer loop.[2,3] The middle bundle starts superiorly to the temporal horn and reaches occipital lobe passing near the inferior occipital fasciculus.[2,3] The posterior bundle runs near the occipital horn and reaches the superior portion of the calcarine fissure.[2,3] Optic radiations emerge from LGNs during VI month of gestation, reaching the occipital cortex under formation.[4] Fast growth of optic radiations was demonstrated before birth, although the final development is reached only after birth, carrying out fibers segregation into visual columns according to ocular dominance.[5] The current literature reports that optic radiations fibers project to the primary (V1), secondary (V2), and tertiary (V3) visual cortices.[6,7]

It is known that LGNs show a very accurate retinotopic map forming three different cellular types: (1) parvocellular layers receiving inputs from cones, (2) magnocellular layers receiving visual signals from rod, and (3) koniocellular cells, which are interspersed between other cells and receive inputs mostly from short wavelength cones.[8]

Optic radiations represent eloquent bundles that need to be investigated (e.g., for presurgical planning of temporal or occipital neoplasms). For this reason, and in order to accurately predict iatrogenic visual deficits,[9] optic radiations are often reconstructed and analyzed by means of magnetic image resonance (MRI)-based diffusion tensor imaging (DTI) tractography,[10,11] From the analysis of anisotropic water diffusion in white matter, this technique permits to reconstruct and visualize the white matter fiber bundles. Although conventional DTI techniques are largely used, several limitations of such approach were demonstrated (i.e., large reconstruction biases and less reliability for fibers with complex configuration; e.g., crossing fibers),[12,13] In order to overcome these limitations, several sequences (and related signal modelling) were developed, like Q-ball imaging and diffusion spectrum imaging (DSI). Although powerful in comparison with DTI, these techniques still suffer from some limitations, such as poor angular resolution for Q-ball[14] and very long acquisition time for DSI.[15] Another modelling technique, known as constrained spherical deconvolution (CSD) has been proven to determine more reliable evaluation of white matter bundles in human brain.[15–17]

The main purpose of this work is to study the optic radiations by means of probabilistic CSD in order to provide a reliable profile of connections in healthy human brains.

Materials and Methods

For this study, sixteen right-handed, healthy subjects (nine males and seven females; age range, 25–40 years; mean age 35) were recruited. All subjects did not suffer from any neurologic disease. The research followed the tenets of the Declaration of Helsinki; informed consent was obtained from the subjects included, after explanation of the nature and possible consequences of the study. The study was approved by the institutional review board of IRCCS Bonino Pulejo, Messina, Italy (Scientific Institute for Research, Hospitalization and Health Care).

Magnetic resonance imaging protocol was performed by means of 3T Achieva Philips MRI (Achieva; Philips Healthcare, Best, The Netherlands) scanner with a 32-channel SENSE head coil (Achieva; Philips Healthcare). For each subject we acquired an anatomical T1-weighted three-dimension (3D) high-resolution Fast Field Echo (field-of-view [FOV] 240$\times$240 mm^2, voxel size 1$\times$1$\times$1 mm, slice thickness 1 mm, flip angle 30°, repetition time (TR) 25 ms, echo time (TE) 4.6 ms) and a diffusion weighted dataset obtained by means of dual-phase encoded pulsed gradient spin echo sequence ($b=1500$ s/mm^2, 64 gradient diffusion directions, FOV 240$\times$240 mm^2 resulting in isotropic 2-mm voxel resolution, TR 11884 ms, TE 54 ms). Subjects motion and movement-by-susceptibility artifacts were corrected by means of unwarp and diffusion toolboxes available for SPM8 package (in the public domain, www.fil.ion.ucl.ac.uk/spm). To this end, a unique reversed phase-encoded b0 image was acquired, for each subject, before diffusion sequence. Rotational part of estimated affine transformations was applied to update gradient diffusion directions. All analyses were performed in native space, following Jones and colleagues,[18] in order to avoid possible misalignment issues.

All regions of interest (ROIs; LGN, V1, V2, V3, V4, and V5) were detected using Juelich probabilistic histologic atlas[19]: First of all, anatomical T1-weighted 3D volumes were nonlinearly coregistered to preprocessed diffusion as previously described.[20] The New Segment Option of SPM8 tool was used to drive the registration procedure comparing cerebro-spinal fluid (CSF) probability maps extracted from T1 and b0 volumes. Usually, an affine mapping of T1s to fractional anisotropy (FA) maps is performed to coregister structural scans to diffusion data. This approach suffers from two inherent flaws: (1) some nonlinear local geometric distortions still persist on diffusion data even after preprocessing, and (2) FA and T1 maps provide different contrasts in brain tissues, because the former is mostly focused on white matter, while the latter mostly highlights gray matter structures. The use of a nonlinear procedure can reduce misregistration by providing a mapping, which more closely follows the anatomy in diffusion space. On the other side, CSF can be extracted with a rather good accuracy both from diffusion data and T1s; thus, spatial priors that are common to both diffusion and T1 spaces can drive CSF-based registration. We know that partial volume effects could affect CSF; for this reason, we used CSF probability maps instead of crude CSF binary ones for warping T1s to diffusion images. This choice allowed performing a weighted registration by further taking into account potential partial volume inaccuracies that might appear in both maps. Coregistered T1s were then normalized to Montreal Neurological Institute (MNI) stereotactic space by means of FSL utilities FLIRT and FNIRT (in the public domain, http://fsl.fmrib.ox.ac.uk/fsl/fslwiki/). Estimated warping fields were later on inverted and applied to Juelich template ROIs in order to have them represented in native space of our subjects. The 50% atlas was used (i.e., only areas that belonged to the claimed structure with a probability $\geq$50% were used). These ROIs were eventually visually inspected by a radiologist with 20 years of experience (MG) and refined to prevent possible misalignments; 3 of 16 subjects showed no more than two spurious voxels in their LGN ROIs (two subjects for left LGN and one subject for the right one), which were erased. Regions of interest correspondent to right and left LGNs were used as seeds for the probabilistic CSD based tractography; all tractographic reconstructions were obtained using MRtrix software package (in the public domain, http://jdtournier.github.io/mrtrix-0.2/index.html).[21] The following reconstruction parameters were used: maximal spherical harmonics degree of 8, maximum fiber length 150 mm, step size 0.2 mm, minimal fiber orientation distribution function (fODF) amplitude 0.15. The latter parameter constitutes a conservative approach that might cause potential underestimation; however, we preferred to use it in order to keep to a minimum false positive tracts,[22] because in this way only voxels with a high probability to belong to white matter are involved in the tracking procedure. Target ROIs were moderately dilated to include gray/white matter boundaries; in this way we ensured that streamlines were able to reach target ROIs for subsequent connectivity analysis. This step could cause an overlapping between different visual area-ROIs (V-ROIs); assigning to a V-ROI those regions that had in the neighborhood, on average, the highest probability of accordance with a specific visual area of the histologic atlas solved these conflicts. All tracts were automatically colored, according to streamlines directions, in green (anterior–posterior direction), blue (cranial–caudal direction), and red (left–right direction). From each LGN, 200,000 streamlines were generated.

For connectivity analysis, we considered the percentage of streamlines ending in each visual area; all calculations were performed by means of in-house scripts built with MATLAB Software Package (in the public domain, www.mathworks.com/products/matlab/), release 2013.

Results

From all the recruited subjects we obtained tractographic reconstructions of right and left optic radiations (Fig. 1). Starting from LGNs, these tracts share the same symmetrical course (Fig. 1A) widely involving occipital lobes. For visualization purposes, each bundle reaching a specific target visual area was manually colored and shown separately (Figs. 1B–F). Average connectivity results are shown in Figure 2. Percentages of LGNs connections with each visual area are distributed as follow (mean % $\pm$ SD): V1 (right 40.88% $\pm$ 3.86; left 54.04% $\pm$ 5.02; average 47.46% $\pm$ 5.50), V2 (right 35.11% $\pm$ 2.88; left 29.78% $\pm$ 4.64; average 32.45% $\pm$ 3.98), V3 (right 10.11% $\pm$ 3.15; left 5.52% $\pm$ 2.67; average 7.81% $\pm$ 3.06), V4 (right 6.03% $\pm$ 2.09; left 2.41% $\pm$ 0.93; average 4.22% $\pm$ 1.82), and V5 (right 7.87% $\pm$ 3.41; left 8.25% $\pm$ 2.63; average 8.06% $\pm$ 2.65). Significant left lateralization was found only for V1 by means of a 2-tailed Wilcoxon rank sum test ($P=0.010$).

Discussion

In this study, we detected and analyzed optic radiations in healthy human brain by means of probabilistic CSD tractography. Our connectivity analysis revealed that the most part of LGN connections mainly involved V1 and V2; however, projections to V3, V4, and V5 were detected. Evidences of

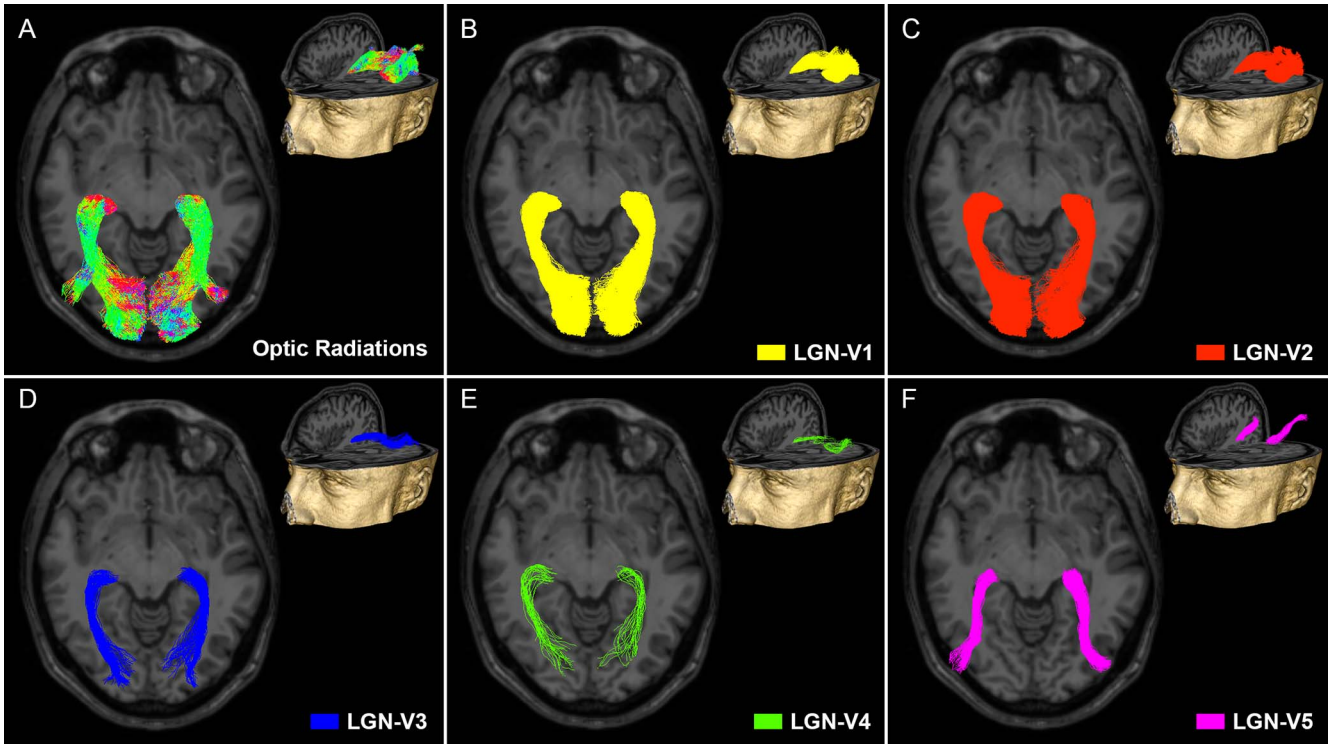

FIGURE 1. (**A**) Tridimensional axial and perspective views of right and left optic radiations in a representative subject. Each bundle was automatically colored according to its main direction. (**B–F**) Tridimensional axial and perspective views of bundles manually colored according to specific visual areas reached (LGN-V1: *yellow*, LGN-V2: *red*, LGN-V3: *blue*, LGN-V4: *green*, and LGN-V5: *magenta*).

strong projections to V1 as well as direct connections to V2 were in keeping with current literature.[7] These projections formed the bulk of the optic radiations structure, hence representing fundamental brain pathways for visual processing. Our connectivity analysis revealed a left lateralization regarding only LGN connections with V1; because all subjects were right-handed, this finding might be related to a left cortical dominance.

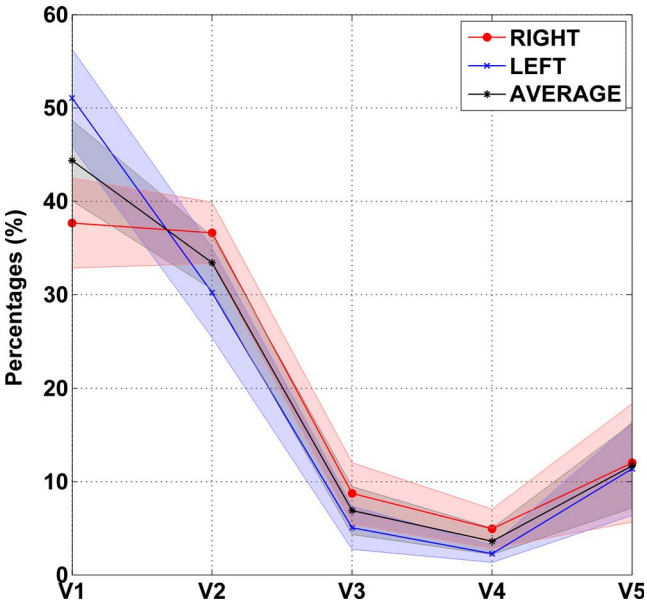

FIGURE 2. Average connectivity analysis of right (*red line*) and left (*blue line*) optic radiations. Percentages of connections with each visual area are distributed as reported in the Results section. Average connectivity profile is further shown with *black line*. *Shaded areas* surrounding each line represent estimated SDs.

In addition to these white matter bundles, growing evidences suggested the hypothesis of a wider involvement in several high order functions of LGN, thus supposing the existence of direct connections with other visual areas. Blindsight (i.e., the phenomenon whereby patients may respond to visual stimuli applied to their blind field)[23] suggested indeed the existence of larger visual connections starting from LGNs. Recently, direct projections to V3 were identified in humans.[6] Our detection of LGN direct connections with V3 were thus in keeping with the findings of Alvarez and colleagues.[6]

To the best of our knowledge, our study was the first showing possible direct LGN-V4 projections in humans. It was demonstrated both in humans and monkeys that V4 area plays a central role in high order functions, spatial attention, and object recognition.[24–26] This area might also contribute to color elaboration[27] as well as depth perception.[28] We knew that tractography is not sufficient to assess per se the existence of a given connection; however, Roe and colleagues' review[29] cited several studies evincing that human V4 might show a similar functional organization to that of monkey, despite functional complexity and specialization differences hold across species. Direct LGN-V4 connections were previously demonstrated to exist in monkeys, following three distinct pathways and respectively involving magnocellular, parvocellular, and koniocellular layers.[30–34] In addition, besides confirming the existence of LGN-V4 connections in macaque brain, Gattass and colleagues[34] further increased V4 functional complexity by proposing that these projections might be bidirectional. Although further functional and dissection

Investigative Ophthalmology & Visual Science

studies are needed, our findings shed new lights on the possible V4 functional skills in human brains.

Lastly, strong LGN connections with V5 were also found in this study. These pathways were previously detected in monkeys by means of tracing studies.[35] In addition, a previous study[36] carried out in a small human cohort, suggested the existence of LGN-V5 pathways; this consideration was supported by the increase of V5 activation following V1 damage, thus suggesting that V5 has an important role for the functional compensation after such damage. Although these findings were also supported by functional studies performed in humans,[37,38] Rabbo and colleagues[39] raised several criticisms about the reliability of these tractographic data. In particular, they argued about several technical limitations of tensor-based models, which might have led to inconsistent DTI evidences of LGN-V5 connection, while suggesting to adopt more advanced approaches. By means of probabilistic CSD-based tractography, a method consistently more reliable than DTI-based one,[15] we were able to support the hypothesis of the existence of a direct LGN-V5 pathway as claimed by Bridge and colleagues.[36] This area was considered as a higher order node for computation and integration of different aspects of visual information, including elaboration of motion and depth perception.[40,41] The existence of direct LGN-V5 connections could provide further possible support for understanding how V5 implements the visual functions.

Our global findings reinforced the hypothesis that LGN network might be the basis both for complex elaboration of visual information as well as the genesis of partially understood visual phenomena, such as blindsight. In the latter case, a recent study demonstrated that LGN could be the key structure for establishing blindsight, because, after injury of V1, it was able to strongly activate other visual areas.[42]

Potential limitations of the present study depended on possible tractography biases; it was essential the use of an adequate signal modelling to achieve highly qualitative results. We wanted to use probabilistic CSD-based tractography, because of its stronger reliability in resolving voxels containing complex fibers configurations.[15] Indeed, it was previously demonstrated that more than 90% of white matter voxels showed fibers with complex geometries (such as crossing fibers).[43] This aspect should be taken into account when reconstructing optic radiations, since their tractographic detection could be affected by the presence of several concurring white matter bundles, like uncinate fasciculus, fronto-occipital fasciculus, superior longitudinal fasciculus, and inferior longitudinal fasciculus.[2,3] To further improve the robustness of our tractographic outcomes we adopted restrictive criteria respecting usual standard,[22,44–46] although we knew we might incur in an underestimation issue. We knew that tractographic findings should be carefully considered[47] because CSD-based tractography, as well as other methods, was not enough to assess real existence of white matter pathways; it rather provided high probability of connection between two regions. Another potential pitfall is related to the possible mislocalization of visual areas. For this study we used a probabilistic atlas; it was, however, known that individual differences might cause inaccuracy in exact ROIs definition. This limitation could be overcome by using fMRI-based localization of visual areas.[48] For these reasons, further studies involving other techniques should be conducted in order to confirm our findings.

In conclusion, we reconstructed optic radiations in healthy humans by means of probabilistic CSD, providing reliable data not affected by tensorial models limitations. We provided LGN complete connectivity profiles, reinforcing the strong evidence of extrastriate LGN connections in human brain. Further studies should be conducted in order to better define functional aspects of all these pathways as well as their possible involvement in functional compensation after occipital lobes damage.

Acknowledgments

Disclosure: **A. Arrigo**, None; **A. Calamuneri**, None; **E. Mormina**, None; **M. Gaeta**, None; **A. Quartarone**, None; **S. Marino**, None; **G.P. Anastasi**, None; **P. Aragona**, None

References

1. Ebeling U, Reulen HJ. Neurosurgical topography of the optic radiation in the temporal lobe. *Acta Neurochir (Wien)*. 1988; 92:29–36.
2. Párraga RG, Ribas GC, Welling LC, Alves RV, de Oliveira E. Microsurgical anatomy of the optic radiation and related fibers in 3-dimensional images. *Neurosurgery*. 2012;71(1 suppl operative):160–171, discussion 171–172.
3. Pujari VB, Jimbo H, Dange N, Shah A, Singh S, Goel A. Fiber dissection of the visual pathways: analysis of the relationship of optic radiations to lateral ventricle: a cadaveric study. *Neurol India*. 2008;56:133–137.
4. Niessen F. Développement des fonctions visuelles du fœtus et du nouveau-né et unites de soins intensifs néonatals. *Arch Pediatr*. 2006;13:1178–1184.
5. Ten Donkelaar HJ, Lammens M, Hori A. *Clinical Neuroembryology Development and Developmental Disorders of the Human Central Nervous System*. Berlin: Springer-Verlag; 2010.
6. Alvarez I, Schwarzkopf DS, Clark CA. Extrastriate projections in human optic radiation revealed by fMRI-informed tractography. *Brain Struct Funct*. 2014;220:2519–2532.
7. Baldwin MK, Kaskan PM, Zhang B, Chino YM, Kaas JH. Cortical and subcortical connections of V1 and V2 in early postnatal macaque monkeys. *J Comp Neurol*. 2012;520:544–569.
8. Solomon SG, Lennie P. The machinery of colour vision. *Nat Rev Neurosci*. 2007;8:276–286.
9. Yogarajah M, Focke NK, Bonelli S, et al. Defining Meyer's loop-temporal lobe resections, visual field deficits and diffusion tensor tractography. *Brain*. 2009;132(pt 6):1656–1668.
10. Kuhnt D, Bauer MH, Sommer J, Merhof D, Nimsky C. Optic radiation fiber tractography in glioma patients based on high angular resolution diffusion imaging with compressed sensing compared with diffusion tensor imaging - initial experience. *PLoS One*. 2013;8:e70973.
11. Cho JM, Kim EH, Kim J, et al. Clinical use of diffusion tensor image-merged functional neuronavigation for brain tumor surgeries: review of preoperative, intraoperative, and postoperative data for 123 cases. *Yonsei Med J*. 2014;55:1303–1309.
12. Jones DK, Cercignani M. Twenty-five pitfalls in the analysis of diffusion MRI data. *NMR Biomed*. 2010;23:803–820.
13. Farquharson S, Tournier JD, Calamante F, et al. White matter fiber tractography: why we need to move beyond DTI. *J Neurosurg*. 2013;118:1367–1377.
14. Tournier JD, Yeh CH, Calamante F, Cho KH, Connelly A, Lin CP. Resolving crossing fibres using constrained spherical deconvolution: validation using diffusion weighted imaging phantom data. *Neuroimage*. 2008;42:617–625.
15. Tournier JD, Calamante F, Connelly A. Robust determination of the fibre orientation distribution in diffusion MRI: non-negativity constrained super-resolved spherical deconvolution. *Neuroimage*. 2007;35:1459–1472.
16. Arrigo A, Mormina E, Anastasi GP, et al. Constrained spherical deconvolution analysis of the limbic network in human, with emphasis on a direct cerebello-limbic pathway. *Front Hum Neurosci*. 2014;8:987.

17. Mormina E, Arrigo A, Calamuneri A, et al. Diffusion tensor imaging parameters' changes of cerebellar hemispheres in Parkinson's disease. *Neuroradiology*. 2014;57:327–334.
18. Jones DK, Catani M, Pierpaoli C, et al. Age effects on diffusion tensor magnetic resonance imaging tractography measures of frontal cortex connections in schizophrenia. *Hum Brain Mapp*. 2006;27:230–238.
19. Eickhoff SB, Stephan KE, Mohlberg H, et al. A new SPM toolbox for combining probabilistic cytoarchitectonic maps and functional imaging data. *Neuroimage*. 2005;25:1325–1335.
20. Besson P, Dinkelacker V, Valabregue R, Thivard L, Leclerc X, Baulac M. Structural connectivity differences in left and right temporal lobe epilepsy. *Neuroimage*. 2014;100:135–144.
21. Tournier JD, Calamante F, Connelly A. MRtrix: diffusion tractography in crossing fiber regions. *Int J Imaging Syst Technol*. 2012;22:53–66.
22. Tournier JD, Calamante F, Connelly A. Effect of step size on probabilistic streamlines: implications for the interpretation of connectivity analysis. *Proc Intl Soc Mag Reson Med*. 2011;19:2019.
23. Riddoch G. On the relative perceptions of movement and a stationary object in certain visual disturbances due to occipital injuries. *Proc R Soc Med*. 1917;10:13.
24. Ungerleider LG, Galkin TW, Desimone R, Gattass R. Cortical connections of area V4 in the macaque. *Cereb Cortex*. 2008;18:477–499.
25. Baluch F, Itti L. Training top-down attention improves performance on a triple- conjunction search task. *PLoS One*. 2010;5:e9127.
26. Saalmann YB, Kastner S. Cognitive and perceptual functions of the visual thalamus. *Neuron*. 2011;71:209–223.
27. Conway BR. Color vision, cones, and color-coding in the cortex. *Neuroscientist*. 2009;15:274–290.
28. Shiozaki HM, Tanabe S, Doi T Fujita I. Neural activity in cortical area V4 underlies fine disparity discrimination. *J Neurosci*. 2012;32:3830–3841.
29. Roe AW, Chelazzi L, Connor CE, et al. Toward a unified theory of visual area V4. *Neuron*. 2012;74:12–29.
30. Ferrera VP, Nealey TA, Maunsell JH. Responses in macaque visual area V4 following inactivation of the parvocellular and magnocellular LGN pathways. *J Neurosci*. 1994;14:2080–2088.
31. Cowey A, Stoerig P. Visual detection in monkeys with blindsight. *Neuropsychologia*. 1997;35:929–939.
32. Rodman HR, Sorenson KM, Shim AJ, Hexter DP. Calbindin immunoreactivity in the geniculo-extrastriate system of the macaque: implications for heterogeneity in the koniocellular pathway and recovery from cortical damage. *J Comp Neurol*. 2001;431:168–181.
33. Soares JGM, Botelho EP, Gattass R. Distribution of calbindin, parvalbumin and calretinin in the superior colliculus and lateral geniculate nucleus of Cebus paella monkeys. *J Chem Neuroanat*. 2001;22:139–146.
34. Gattass R, Galkin TW, Desimone R, Ungerleider LG. Subcortical connections of area V4 in the macaque. *J Comp Neurol*. 2014;522:1941–1965.
35. Sincich LC, Park KF, Wohlgemuth MJ, Horton JC. Bypassing V1: a direct geniculate input to area MT. *Nat Neurosci*. 2004;7:1123–1128.
36. Bridge H, Thomas O, Jbabdi S, Cowey A. Changes in connectivity after visual cortical brain damage underlie altered visual function. *Brain*. 2008;131:1433–1444.
37. Bridge H, Hicks SL, Xie J, et al. Visual activation of extra-striate cortex in the absence of V1 activation. *Neuropsychologia*. 2010;48:4148–4154.
38. Gaglianese A, Costagli M, Bernardi G, Ricciardi E, Pietrini P. Evidence of a direct influence between the thalamus and hMT+ independent of V1 in the human brain as measured by fMRI. *Neuroimage*. 2012;60:1440–1407.
39. Rabbo AF, Koch G, Lefèvre C, Seizeur R. Direct geniculo-extrastriate pathways: a review of the literature. *Surg Radiol Anat*. 2015;37:891–899.
40. Born RT, Bradley DC. Structure and function of visual area MT. *Annu Rev Neurosci*. 2005;28:157–189.
41. Zeki S. Area V5-a microcosm of the visual brain. *Front Integr Neurosci*. 2015;9:21.
42. Schmid MC, Mrowka SW, Turchi J, et al. Blindsight depends on the lateral geniculate nucleus. *Nature*. 2010;466:373–377.
43. Jeurissen B, Leemans A, Tournier JD, Jones DK, Sijbers J. Investigating the prevalence of complex fiber configurations in white matter tissue with diffusion magnetic resonance imaging. *Hum Brain Mapp*. 2013;34:2747–66.
44. Descoteaux M, Deriche R, Knösche TR, Anwander A. Deterministic and probabilistic tractography based on complex fibre orientation distributions. *IEEE Trans Med Imaging*. 2009;28:269–286.
45. Milardi D, Bramanti P, Milazzo C, et al. Cortical and subcortical connections of the human claustrum revealed in vivo by constrained spherical deconvolution tractography. *Cereb Cortex*. 2015;25:406–414.
46. Milardi D, Gaeta M, Marino S, et al. Basal ganglia network by constrained spherical deconvolution: a possible cortico-pallidal pathway? *Mov Disord*. 2015;30:342–349.
47. Jbabdi S, Johansen-Berg H. Tractography: where do we go from here? *Brain Connect*. 2011;1:169–183.
48. Henriksson L, Karvonen J, Salminen-Vaparanta N, Railo H, Vanni S. Retinotopic maps, spatial tuning, and locations of human visual areas in surface coordinates characterized with multifocal and blocked FMRI designs. *PLoS One*. 2012;7:e36859.

Investigative Ophthalmology & Visual Science